After-pulsing and cross-talk comparison for KETEK PM1125NS-SB0, Hamamatsu S10362-11-100C and Hamamatsu S13360-3050CS.

1. Abstract

Silicon photomultipliers (SiPM) have become widespread recently. They exceed photomultipliers on quantum efficiency, size and resistance to the magnetic field. However, due to the features of the structure they have a greater value of dark noise, as well as have additional sources of noise: cross-talk and after-pulsing. In addition, these parameters may have a temperature dependence.

In this article we study dark noise, probabilities of cross-talk and after-pulsing at different voltages and temperatures for two modern SiPM: Hamamatsu S13360-3050CS and KETEK PM1125NS-SB0 and Hamamatsu S10362-11-100C SiPM from the previous generation. An offline signal processing was performed by a pulse approximation with reconstruction of amplitudes and start times to find these parameters. As a result, we found that in achieved measurement accuracy dark noise has a temperature and a voltage dependence, but cross-talk and after-pulsing probabilities have only the latter.

Measured cross-talk probabilities for KETEK PM1125NS-SB0 and Hamamatsu S13360-3050CS at their operating voltage is about 6% which is two times smaller than that for Hamamatsu S10362-11-100C. The total after-pulsing probability (fast component) for KETEK PM1125NS-SB0 and Hamamatsu S13360-3050CS is about 12%, which is also almost 2 times smaller than that for Hamamatsu S10362-11-100C (fast and slow component). Dark noise rate for Hamamatsu S13360-3050CS at 20 $°C$ is only 30 kHz/mm^2 in comparison with 80 kHz/mm^2 for KETEK PM1125NS-SB0.

2. Introduction

BINP many years engaged in the development of X-ray inspection systems [1]. These installations can be used in various fields: inspection at airports, subways or at workplaces. Multistrip ionization chamber filled with pure Xe at 15 bar have been used as X-ray detector until now. However, this detector has a serious disadvantage - it works in the integrating mode, so at low input flow of particles electronic noise seriously degrades quality of images. Another disadvantage is the insufficiently high detection efficiency of high-energy photons. In this regard, it was decided to choose a new detector based on SiPM and a scintillator which may have a detection efficiency > 90 % and operate in the mode of direct photon counting.

The main purpose of this work is to measure after-pulsing and cross-talk probabilities for two SiPM: KETEK PM1125NS-SB0 and Hamamatsu S13360-3050CS and compare

them with characteristics of Hamamatsu S10362-11-100C - the device from previous generation.

3. Measurement of breakdown voltage

One of important characteristics of any SiPM is a breakdown voltage. A breakdown voltage V_{BD} is a voltage at which a gain equals to zero.

In many works are shown that various SiPMs gain is a linear function of both a temperature and a voltage. Thus, the expression for a gain $G(V,T)$ is written as follows: [2–5]:

$$G(V,T) = a \cdot V + b \cdot T + c \qquad (1)$$

It is easy to find a breakdown voltage equating the gain from Eq.(1) to zero :

$$V_{BD}(T) = \frac{-(b \cdot T + c)}{a} = \frac{dV}{dT} \cdot T + const \qquad (2)$$

The following installation was assembled for measurement of a breakdown voltage and a gain (Fig. 1). The light source based on fast LED (CAEN SP5601) sends a flash through an optical fiber to SiPM. At the same time, the light source sends a trigger signal to the CAEN DT5720A ADC. The signal from the SiPM passes through the amplifier to the CAEN DT5720A, which integrates the signal in the presence of the trigger signal. The resulting charge is transmitted to computer in on-line mode. SiPM is mounted on a thermoelectric cooler and the temperature stabilization is ensured by the TRM 101 PID controller. The deviation from the set temperature does not exceed 1K.
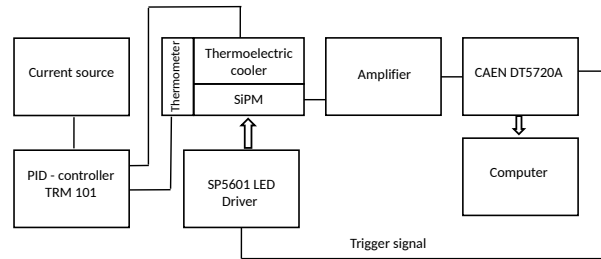

Рис. 1. The Installation scheme for measurement the SiPM breakdown voltage.

The calculation of the breakdown voltage had several stages. The intensity of the light source was set so that there were not SiPM triggering or single photon was registered in generally. The signal was integrated into the gate with 200 ns duration ($\approx 5 \cdot \tau$). Then the tops of the noise peak and the peak from the registration of single photons were approximated by a Gaussian function. We calculated the distance Δ

between the 0th and the 1st peak. Distances between the first and the second, the second and the third etc. peaks were not considered. The main reason was that as the number of peak increased the greater became the discrepancy between the true and measured peak position because of after-pulses. An example of charge spectrum is shown in Fig. 2. In measurements an voltage error ΔV was estimated at 0.01 V, and a temperature error ΔT was estimated as the minimum temperature step 1 K divided by $\sqrt{12}$.
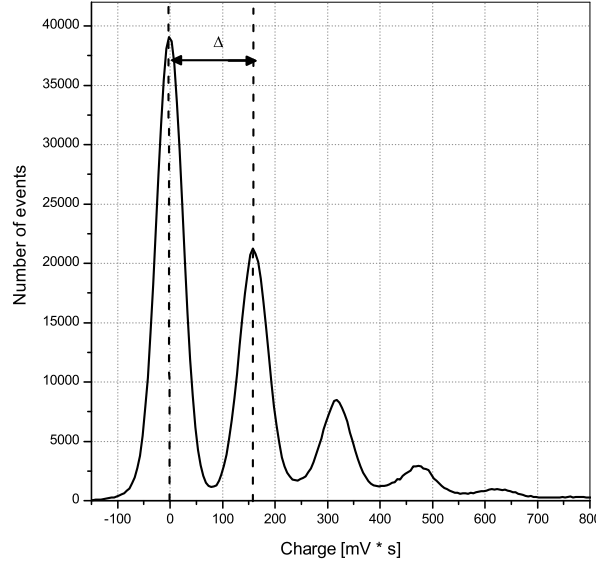

Рис. 2. Spectrum from Hamamatsu S13360-3050CS at 71 V voltage and 270 K temperature under irradiation by LED. The integration time is 300 ns.

The value Δ associated with a gain as follows:

$$G = \Delta \cdot ADC_{\text{conversion rate}}/\text{charge of electron},$$

where $ADC_{\text{conversion rate}}[C/(mV{\cdot}s)]$ - a conversion coefficient. To determine the conversion coefficient a rectangular pulse from generator was sent to the test input of the amplifier through the capacitance $C = 1pF$. After tract calibration all measurements $G(V, T)$ were approximated by Eq.(1) to find a, b, c parameters. Then using Eq.(2) we found the dependence of a breakdown voltage on a temperature.

4. Cross-talk and after-pulsing probabilities finding algorithm

4.1. Theory

There are several algorithms for finding cross-talk probabilities. One of them is described in [6]. The idea is to measure dark noise rate at different thresholds. A cross-talk probability can be defined as the ratio of the rates with 1.5 photoelectrons(phe)

and 0.5 photoelectrons threshold:

$$P_{X-talk} = \nu_{1.5phe}/\nu_{0.5phe} \tag{3}$$

However, this method has a significant disadvantage: after-pulses are indistinguishable from cross-talk if the former above a threshold. Furthermore, this algorithm does not use information about a signal form, which makes the frequency dependence of the threshold more blurred and complicates the finding of the $\nu_{1.5pe}$ value.

An advanced algorithm should use the information about a waveform. There are two approaches to signal processing: inverse convolution [7] and an approximation of the original signal [8–10]. In this article we decided to use the method of signal approximation, because it is described in more detail in the above works.

In the process of approximation we obtain amplitudes and start times of signals. Using this information we recover the time constants and probabilities for after-pulses.

After-pulsing is repeated triggering of a cell, which occurs in some time moment after it is triggering. The reason of after-pulsing is a capture of electrons into traps during an avalanche and their subsequent release after a time interval from a few nanoseconds to several microseconds [6]. After triggering of the primary signal a voltage in a cell decreases to a breakdown voltage and then will recover to its original value exponentially:

$$V(\Delta t) = V_{BD} + \Delta V \cdot (1 - \exp{(-\Delta t/\tau_{rec})}), \tag{4}$$

where V_{BD} - a SiPM breakdown voltage, ΔV - an overvoltage ,τ_{rec} - a recovery time of a cell.

There are several processes, which may cause of a cell retriggering. First of all, it is after-pulsing. Because of different physical mechanisms of electron traps, there are two types of after-pulses: fast and slow [8–10]. Secondly, dark noise may cause of a cell retriggering. Each of the two processes has exponential time distribution with its own time constant τ:

$$f(\Delta t) = \frac{1}{\tau} \cdot \exp(-\Delta t/\tau), \tag{5}$$

where τ - an average time elapsing between two pulses when considering only one of the above effects. Measuring distances between signals we build pulse interval spectrum. Then we approximate the probability density of the pulse interval by an analytic function. Function parameters characterize time constants and probabilities of processes leading to the triggering.

Since we are interested in the pulse interval density, it is necessary to know the probability $P(t)$ that on the interval from 0 to t pulses can't exist and on the interval from t to $t + \delta t$ must occur one pulse. If we consider only one exponential process, this probability is $P_{exp}(t) = \nu \cdot e^{-t \cdot \nu} \cdot \delta t \ (t = 1/\nu)$.

We deduce the pulse interval density, if dark pulses or after-pulses can occur in a cell. For a start, consider the case when there are after-pulses only one type, occurring with a p probability and a ν frequency. Dark pulses, as well as after-pulses have an exponential distribution (5). Since dark pulses are independent of after-pulses the required probability $P(t)$ can be written as follows:

$$P(t) = P\{\text{there are not after-pulses from 0 to } t + \delta t\} \cdot P\{\text{there is dark pulse from } t \text{ to } t + \delta t\} + \quad (6)$$
$$P\{\text{there is after-pulse from } t \text{ to } t + \delta t\} \cdot P\{\text{there are not dark pulses from 0 to } t + \delta t\}$$

The contribution of each process is as follows:

$$P\{\text{there are not after-pulses from 0 to } t + \delta t\} = (1 - p) + p \cdot e^{-\nu \cdot t} \qquad (7)$$
$$P\{\text{there is dark pulse from } t \text{ to } t + \delta t\} = (\nu_{dc} \cdot e^{-\nu_{dc} \cdot t}) \cdot \delta t$$
$$P\{\text{there is after-pulse from } t \text{ to } t + \delta t\} = p \cdot (\nu \cdot e^{-\nu \cdot t}) \cdot \delta t$$
$$P\{\text{there are not dark pulses from 0 to } t + \delta t\} = e^{-\nu_{dc} \cdot t}$$

Thus, substituting probabilities in Eq.(6) from Eq.(7) and reducing the resulting expression on δt we obtain the probability density of pulse intervals:

$$f(t) = p \cdot (\nu + \nu_{dc}) \cdot e^{-(\nu + \nu_{dc}) \cdot t} + (1 - p) \cdot \nu_{dc} \cdot e^{-\nu_{dc} \cdot t} \qquad (8)$$

It is worth noting that a similar formula is given in [10], but with a typo in the sign between the terms.

As a result, taking into account the fast and slow component of after-pulses and dark noise the probability density distribution of pulse intervals can be written as follows:

$$f(t) = p_s \cdot p_f \cdot (\nu_s + \nu_f + \nu_{dc}) \cdot e^{-(\nu_s + \nu_f + \nu_{dc}) \cdot t} + \qquad (9)$$
$$p_s \cdot (1 - p_f) \cdot (\nu_s + \nu_{dc}) \cdot e^{-(\nu_s + \nu_{dc}) \cdot t} +$$
$$p_f \cdot (1 - p_s) \cdot (\nu_f + \nu_{dc}) \cdot e^{-(\nu_f + \nu_{dc}) \cdot t} +$$
$$(1 - p_s) \cdot (1 - p_f) \cdot \nu_{dc} \cdot e^{-\nu_{dc} \cdot t}$$

Eq.(9) is valid if the measured distance between the signals caused by the triggering of a single cell. Signals caused by the simultaneous triggering of two or more cells (because of cross-talk) should not be considered in obtaining the probability density of pulse intervals.

In the article [9] shown another result for the probability density of pulse intervals which differ from that obtained in this work. This is due to the consideration of one more

process - delayed crosstalk. However, in practice the probability of delayed crosstalk is much lower than the probability of direct cross-talk, and in our experiments we did not observe it. The information about other processes that are responsible for a cell triggering can be found in [11].

4.2. Signal finder

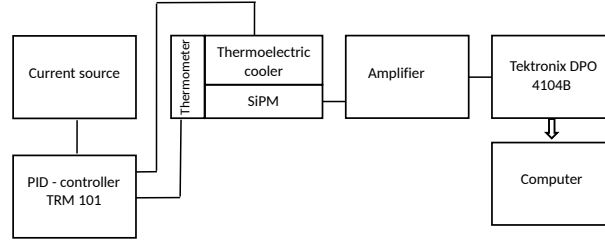An installation scheme for recording SiPM signals is shown in Fig.3.

Рис. 3. The installation scheme for recording SiPM signals.

Data in raw format were recorded on a computer using the oscilloscope Tektronix DPO 4104B. The trigger was disabled during the recording. The continuous recording length was 5MSamples at a digitizing frequency equal to 5GHz. For each voltage and temperature on SiPM were recorded 1000 files, i.e. one second of a signal.

The signal from the SiMP can be presented as the sum of single-electron pulses $Signal_{1e}(t - t_i)$ with a random amplitude A_i and a start time t_i:

$$V(t) = \sum_{i=0}^{N} A_i \cdot Signal_{1e}(t - t_i) + V_0 \tag{10}$$

The waveform of the single-electron pulse was found from the analysis of the recorded signal and was approximated by an analytical function. The recorded signal was processed by a special algorithm that found single-electron pulses without after-pulses impurities and averaged them. Signals with after-pulses were thrown out in order to find the correct waveform. The waveform of the single-electron pulse for different SiPM is shown in Fig.4. The waveform was measured at different overvoltages and temperatures (from -8 to 27 $°C$), but one remained practically unchanged.

Further, single-electron pulses were approximated by function obtained from the convolution of Eq.(11) with a Gauss distribution describing the contribution of the limited operating speed of electronics. The Result of a convolution is shown in Eq.(12), where σ is the standard deviation of the Gauss distribution.

$$V(t) = A \cdot \exp\left[-\frac{t - t_0}{\tau_{rec}}\right] \cdot \left(1 - \exp\left[-\frac{t - t_0}{\tau_{rise}}\right]\right) \cdot \theta(t - t_0) + V_0, \tag{11}$$
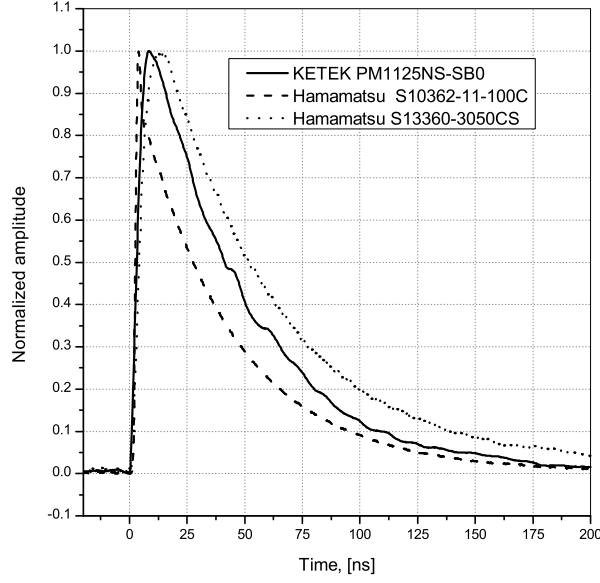
6

Рис. 4. The waveform of the single-electron pulse from different SiPMs.

where A - a pulse amplitude, t_0 - a time delay, τ_{rec} - a recovery time of a cell, τ_{rise} - a rise time of a rising edge, V_0 - a voltage shift, $\theta(t - t_0)$ - the Heaviside step function.

$$V(t) = V_0 + \frac{A}{2} \cdot \left(\{F(\sigma, \tau_{rec}) - F(\sigma, \tau_{total})\} \right), \text{ where} \tag{12}$$

$$F(\sigma, \tau) = \exp\left[\frac{\sigma^2 - 2t \cdot \tau}{2\tau^2}\right] \cdot \left(1 + Erf\left[\frac{t - \sigma^2/\tau}{\sigma\sqrt{2}}\right]\right),$$

$$\tau_{total} = \frac{\tau_{rec} \cdot \tau_{rise}}{\tau_{rec} + \tau_{rise}}$$

A further task was to find A_i, t_i parameters as well as the N parameter. The N parameter characterizes the number of signals are represented in a data fragment. A file can be divided into multiple independent parts, each of which describes a signal according to the Eq.(10) at different N parameters. A C ++ program was written to process raw data.

The main problem with processing is the presence of noise. There are a lot of digital filters that can smooth a signal, but their use will lead to loss of the information about after-pulses. After-pulses are exponentially distributed in time and with a high probability they occur at short times, when a cell voltage has not yet recovered.

However, an accuracy of signals location can be improved if we transmit into the approximation algorithm initial parameters close to true ones. For this purpose a signal derivative was calculated with the simultaneous smoothing (The Savitsky-Golay third-order filter with the number of points equal to 51 (10.2 ns)) Thus, the information about the derivative was also involved in the processing.

To split a recorded file into multiple independent signals, we used the following

7

algorithm:

1) The first derivative was calculated using the Savitsky-Golay filter.

2) If the derivative and an amplitude was higher of threshold values th_{der} and th_{amp}^{start} then the time 20 ns before this event was taken as the time of the start signal. This condition was necessary for the proper calculation of a basic line of a signal. Otherwise, a falling edge from a previous signal distort the baseline.

3) If after the previous step passed more than 5 ns and the signal level was below the threshold amplitude th_{amp}^{stop} and ahead on 20 ns the derivative was below the threshold th_{der}, then this time was the end time of the signal. The amplitude threshold th_{amp}^{stop} was chosen as the intersection of the signal with the baseline.

To determine th_{amp}^{start} we drew the dependence of events number from the threshold at different values of the dead time τ_{amp}^{dead}. An example is shown in Fig. 5 for Hamamatsu S10362-11-100C at $T = 295K$ and $\Delta V = 1V$. The threshold for triggering by amplitude th_{amp}^{start} was chosen at half amplitude of the single-electron signal and corresponded approximately to $0.02V$ The thresholds was practically independent of the selected dead time τ_{amp}^{dead}.

A similar graph can be drawn for the derivative (Fig. 6). We selected only those signals that exceed the amplitude threshold $th_{amp}^{stop} = 0.002V$. Without this condition the graph would be significantly distorted because noise can have a derivative is comparable to a signal derivative. Above the threshold $4 \cdot 10^{-4}V/s$ the contribution of noise is significantly suppressed. This value is selected as th_{der}. However, thresholds th_{der} and th_{amp}^{start} are other for other overvoltages.

As a result of this algorithm data files were divided into multiple independent parts. At each part can be either one pulse or many pulses.

4.3. Correlation analysis

To find parameters A_i and t_i each part have to be approximated by Eq.(10). This function internally nonlinear on the t_i parameter therefore it is necessary to set the initial parameter of the start time of a signal. To do this, we used the following algorithm:

1) If the first derivative was above the threshold, then we were looking for a derivative maximum from a current time to a current time plus 5 ns. The time at which the first derivative reached the maximum used as the initial value of the t_i parameter.

2) If the first derivative was below the threshold value and passed more than 5 ns then was allowed to search for the next threshold exceeding.

Further, an each independent part was approximated by Eq.(10) at $N = 1$. Consider the correlation between the amplitude and χ^2/Dof (Fig. 7). One can notice a few
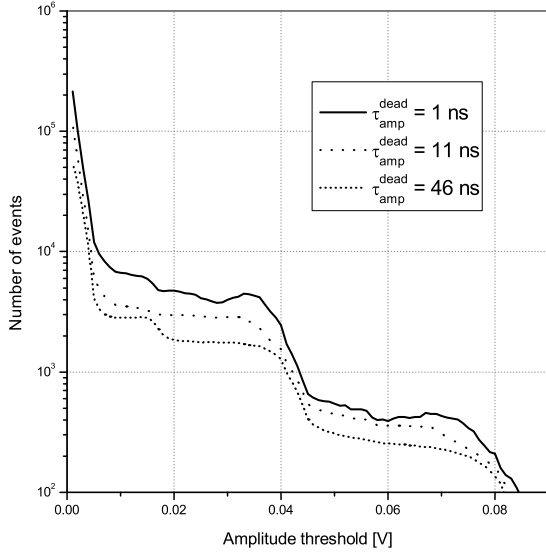
Рис. 5. The dependence of the number of found signals from the amplitude threshold and the dead time τ_{amp}^{dead} for Hamamatsu S10362-11-100C at 1V overvoltage and 295K temperature.
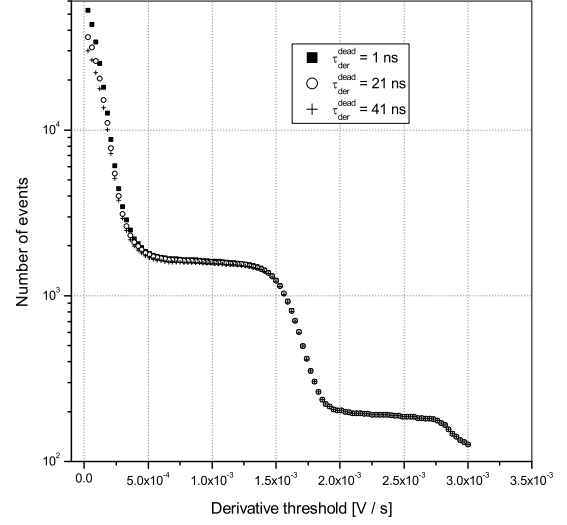

Рис. 6. The dependence of the number of found signals from the derivative threshold and the dead time τ_{der}^{dead} for Hamamatsu S10362-11-100C at 1V overvoltage and 295K temperature. Only signals exceeding the threshold $th_{amp}^{stop} = 0.002V/s$ were selected.

outlying clusters: A_1, B_1, C_1 etc. The cluster A_1 corresponds to single-electron signals. Clusters B_1, C_1 etc. corresponds to events when simultaneously triggered two, three or more cells (cross-talk), and these signals was located away from other signals. Because of this they have the low χ^2/Dof value at the approximation of a single-component function. Other events with the $\chi^2/Dof > 4$ value (we denote them as Z_1 cluster) correspond to several signals, located at a relatively short distance distance from other.

In the next step the events from the Z_1 cluster were approximated by Eq.(10) at $N = 2$. In that case, each event is characterized by four parameters: χ^2/Dof, amp_1 and amp_2 - amplitudes of the first and the second signals, Δt - a distance between the signals. Draw a correlation between the total amplitude $amp_1 + amp_2$ and a χ^2/Dof value (Fig. 8).

In this case also there are several typical clusters: A_2, B_2, C_2 etc. A more clear idea about the signals forming these clusters can be obtained from the correlation of $amp_1 + amp_2$ and Δt constructed for a particular cluster (Fig. 9 and Fig. 10).

The $A2$ cluster consists of signals that are conventionally divided into two sets: α_1 и β_1. The set α_1 corresponds to two closely spaced signals and their total amplitude equal to double amplitude of the single-electron pulse. This means that these signals
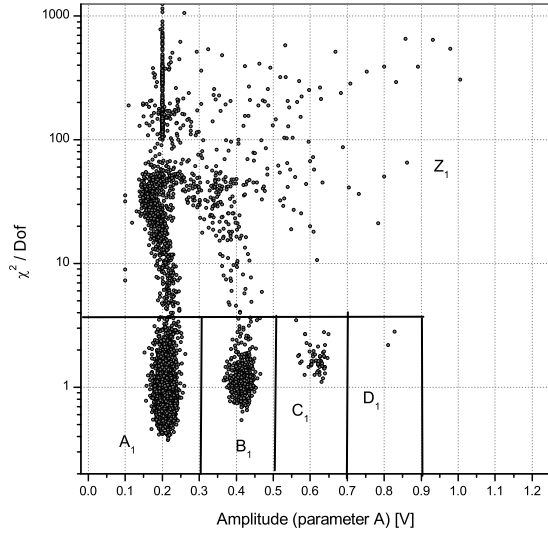
Рис. 7. The correlation between the total amplitude $amp_1 + amp_2$ and χ^2/Dof when approximating all pulses by one-component function. The signal was obtained from Hamamatsu S10362-11-100C at 1V overvoltage and 295K temperature.
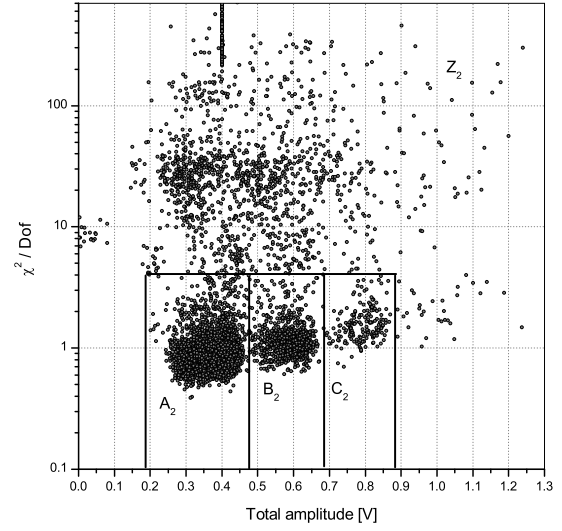
Рис. 8. The correlation between the total amplitude $amp_1 + amp_2$ and χ^2/Dof when approximating the Z_1 cluster (see Fig. 7) by two-component function. The signal was obtained from Hamamatsu S10362-11-100C at 1V overvoltage and 295K temperature.

were caused by triggering of various cells and they are dark noise. At the same time signals from the set β_1 have an amplitude that depends on the distance between signals. This means that the first signal was a single-electron signal and the subsequent signal was an after-pulse. The similar correlation can be constructed for the B_2 set (Fig. 10). In this case, the set α_2 consists of two closely spaced signals one of which has a single-electron amplitude. Another signal has the double amplitude caused by the simultaneous triggering of two cells due to cross-talk.

The set β_2 contains signals that can be divided into two groups. The first group was formed by signals in which two cells triggered simultaneously and then one of cells generated an after-pulse. The second group was formed by signals in which one cell triggered and then after-pulse occurred which caused cross-talk. The sets similar to A_2 and A_2 with a large total amplitude correspond to the events with a greater number of simultaneously triggered cells.

Then we built pulse interval spectrum. We took into account only the signals without cross-talk, i.e. we measured the distance only between those signals that belong to the A_1 or A_2 clusters. In the first approximation we can neglect events in the A_3, A_4 etc. clusters due to their small number relative to events in the A_1 or A_2 clusters.

As a result, we obtained the pulse interval spectrum shown in Fig. 11. By approximating
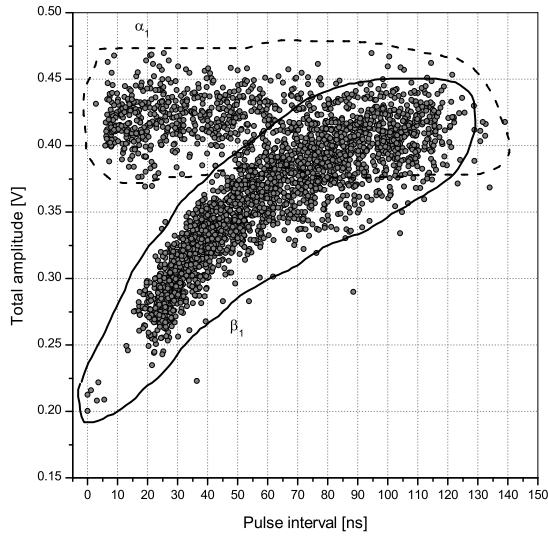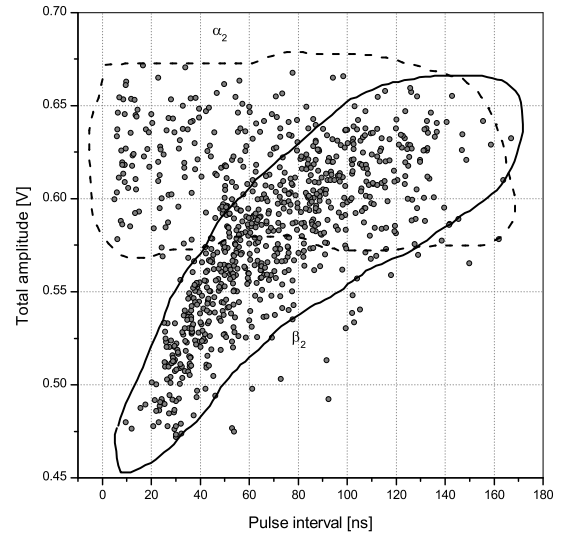
10

Рис. 9. The correlation between the pulse interval and the total amplitude when approximating the A_2 cluster (see Fig. 8) by two-component function. The signal was obtained from Hamamatsu S10362-11-100C at 1V overvoltage and 295K temperature.

Рис. 10. The correlation between the pulse interval and the total amplitude when approximating the B_2 cluster (see Fig. 8) by two-component function. The signal was obtained from Hamamatsu S10362-11-100C at 1V overvoltage and 295K temperature.

the spectrum by Eq.(9) we found p_s, p_f, ν_s, ν_f, ν_{DC} parameters. For the approximation RooFit package and unbinned fit were used.

As you can see there is a change in the spectrum monotony when the pulse interval equals approximately 25 ns. If the after-pulse occurs with the pulse interval less than 25 ns after the previous pulse, its amplitude is small and this pulse cannot be distinguished from noise. Because of this the signal is recognized as a single component and it does not contribute to the short times. This distorts the spectrum. For the correct approximation we took into account only pulse intervals exceed a certain "threshold"value. To clarify this value approximation was performed at different threshold values. The dependence of the τ_f parameter from the pulse interval threshold is shown in Fig. 12. For this type of SiMP at 295K temperature and 1V overvoltage 25 ns threshold was chosen. When reducing the overvoltage the pulse interval threshold increases.
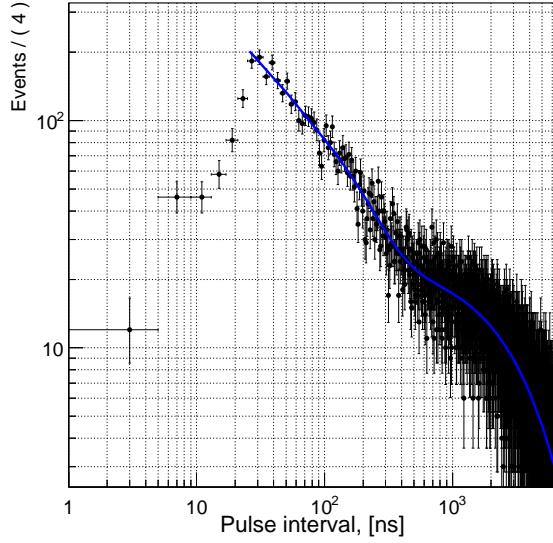
Рис. 11. The pulse interval spectrum approximated by Eq.(9). Events with cross-talk are not taken into account. The signal was obtained from Hamamatsu S10362-11-100C at 1V overvoltage and 295K temperature.
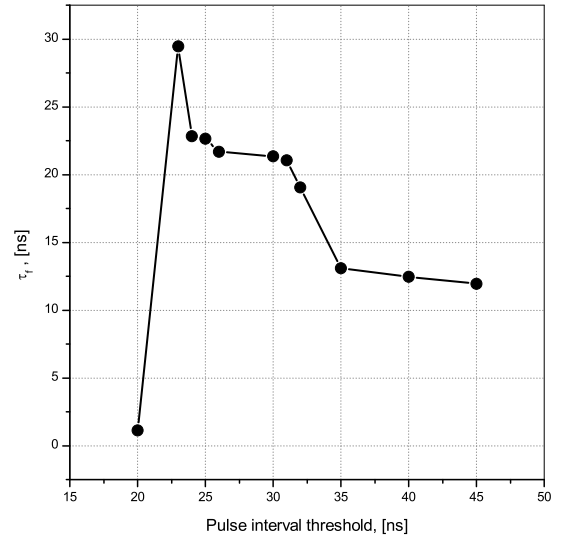

Рис. 12. The dependence of the after-pulse fast component from the pulse interval threshold. The signal was obtained from Hamamatsu S10362-11-100C at 1V overvoltage and 295K temperature.

5. Results

5.1. Dark noise

As the result of the approximation of the pulse interval spectrum the dependence of dark noise rate on a temperature and an overvoltage were obtained (Fig.13, 14, 15, 16). The dependence of dark noise rate on a temperature is expressed by the following formula [4]:

$$\nu(\Delta V = const, T) = A \cdot T^{3/2} \cdot \exp\left[-\frac{E_g}{2k_B \cdot T}\right], \tag{13}$$

where A is a constant, depending on a voltage, the material and technological parameters, T is an absolute temperature, E_g is a bandgap, k_B is the Boltzmann constant. The dependence of dark noise rate on an overvoltage is expressed by the linear law:

$$\nu(\Delta V, T = const) = k \cdot \Delta V \tag{14}$$

However we were failed to collect enough statistics for data approximation in this manner for Hamamatsu S13360-3050CS because of its low noise level. For the same reason, only one point at the maximum noise level was obtained for KETEK PM1125NS-SB0.

12
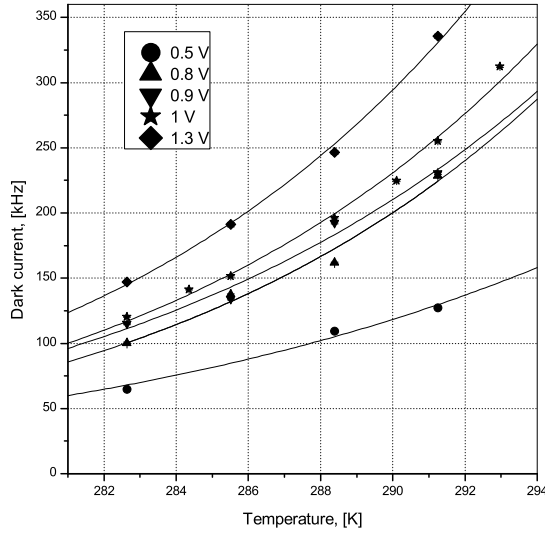
Рис. 13. The dependence of dark noise rate on a temperature at a fixed overvoltage for Hamamatsu S10362-11-100C. The data were approximated by Eq.(13).
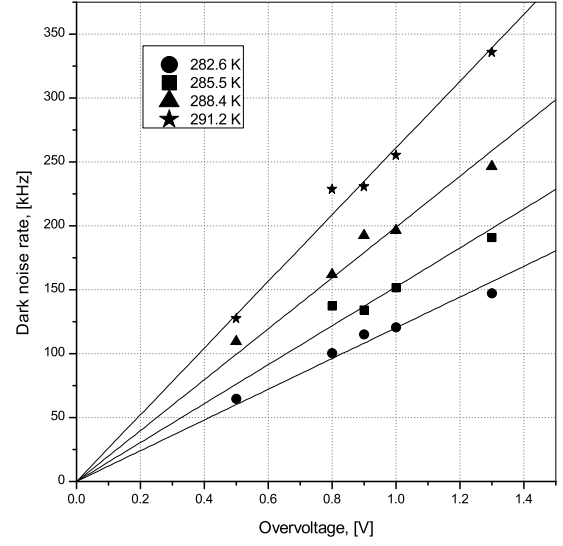
Рис. 14. The dependence of dark noise rate on a overvoltage at a fixed temperature for Hamamatsu S10362-11-100C. The data were approximated by Eq.(14).

5.2. Cross-talk

The A_1 cluster (Fig. 7) consists of single-electron pulses. The B_1 cluster consists of pulses caused by the simultaneous triggering of two cells. The C_1 cluster consists of pulses caused by the simultaneous triggering of three cells. The A_2 cluster (Fig. 8) consists of pulses caused by triggering of one cell with the subsequent after-pulse or triggering two cells at different time points because of dark noise. The B_2 cluster consists of pulses caused by the simultaneous triggering of two cells with the subsequent after-pulse of one of the cells or triggering of one cell with the subsequent after-pulse, causing cross-talk.

At the moment, we calculate the cross-talk probability as follows:

$$P_{X-talk} = (N_{B_1} + N_{C_1})/(N_{A_1} + N_{B_1} + N_{C_1}) \qquad (15)$$

This is an approximate formula because one should take into account the fact that a small part of with cross-talk events is contained in B_2, C_2, B_3, C_3, etc. clusters.

The cross-talk probability should have the quadratic dependence of an overvoltage in the first approximation. This is explained by the cross-talk probability P_{x-talk} is proportional to the number of electrons in the avalanche G and the triggering probability of cells by photon ε_{Geiger}. G and ε_{Geiger} have a linear dependence on an overvoltage(for ε_{Geiger} value the dependence differs from linear at a high overvoltage
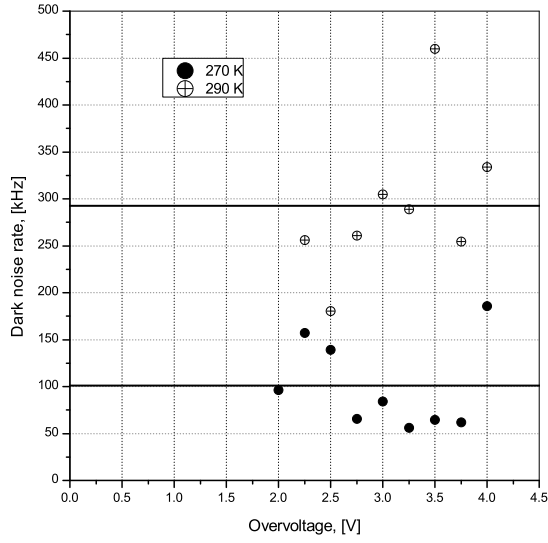
Рис. 15. The dependence of dark noise rate on a overvoltage at a fixed temperature for Hamamatsu S13360-3050CS. Lines are approximation of the data by constant for different temperatures.
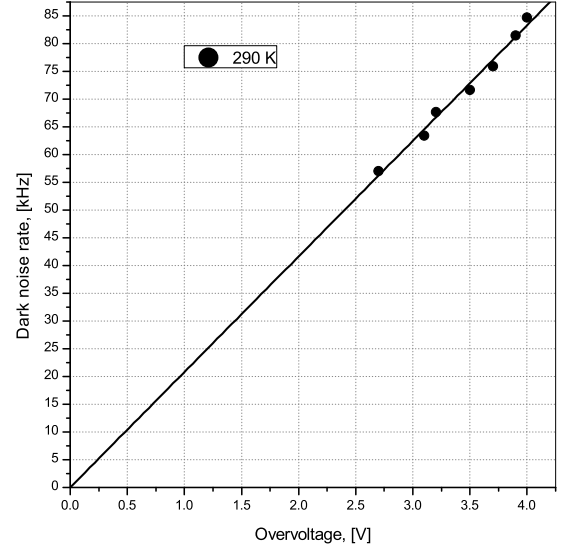

Рис. 16. The dependence of dark noise rate on a overvoltage at a fixed temperature for KETEK PM1125NS-SB0. The line is approximation of the data by linear function.

[12]):

$$P_{x-talk}(\Delta V) \propto G(\Delta V) \cdot \varepsilon_{Geiger}(\Delta V) \tag{16}$$

Thus, the experimental data were approximated by the following formula:

$$P_{x-talk}(\Delta V, T) = k_{x-talk} \cdot \Delta V^2 \tag{17}$$

The results of processing are shown on Fig. 17, 18, 19, 20.

Based on the experimental data, it can be concluded that the cross-talk probability is temperature independent.

5.3. Checking the model of four nearest neighbors

It noted the existence of SiPM, which do not correspond to the model of four nearest neighbors [7]. In the model of four nearest neighbors it is assumed that a trigged cell can cause the triggering of only four nearest cells. In this case, the cross-talk probability in the next cell p is related to the full cross-talk probability P_{x-talk} by the following equation

$$(1-p)^4 = 1 - P_{X-talk} \tag{18}$$

14
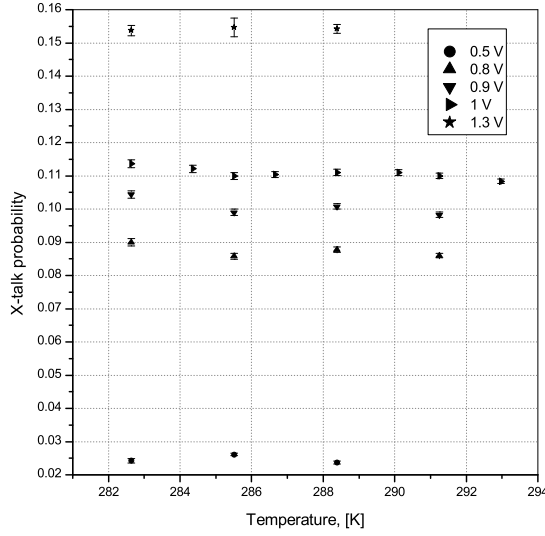
Рис. 17. The dependence of the cross–talk probability on a temperature at a fixed overvoltage for Hamamatsu S10362-11-100C.
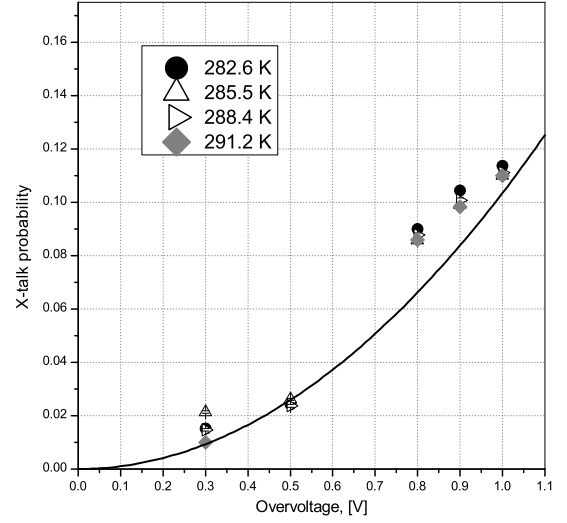
Рис. 18. The dependence of the cross–talk probability on a overvoltage at a fixed temperature for Hamamatsu S10362-11-100C. The data were approximated by a quadratic function.

The full cross-talk probability was calculated by the Eq.(15). Then the p value was calculated by Eq.(18). It was calculated the theoretical probability that due to cross-talk only one cell triggered [7]: $p_{2phe}^{theory} = 4 \cdot p \cdot (1 - p)^6$. On the other hand it was calculated the experimental probability p_{2phe}^{exp} as the ratio of events number $N_{2p.e.}$ to the total number of events, where $N_{2p.e.} \approx N_{B_1}/(N_{A_1} + N_{B_1} + N_{C_1})$. As a result of measurements, it was found that the ratio $p_{2phe}^{exp}/p_{2phe}^{theory}$ for Hamamatsu S10362-11-100C varies from 1 to 1.08 depending on a temperature and an overvoltage, and for Hamamatsu S13360-3050CS and KETEK PM1125NS-SB0 this ratio varies from 0.98 to 1.02. Thus it can be concluded that the model of four nearest neighbors works well for considered SiPMs.

5.4. After-pulses

As a result of spectrum approximation we fond also probabilities and time constants for after-pulses. The obtained data are shown in Fig. 21, 22, 23, 24, 25, 26, 27, 28, 29, 30, 31, 32.

After-pulse probabilities p_s and p_f at the current accuracy of the measurement are independent of a temperature. At the same time, this probabilities have to have a quadratic dependence on an overvoltage:

$$p_i(\Delta V, T) = k_i^p \cdot \Delta V^2 \tag{19}$$
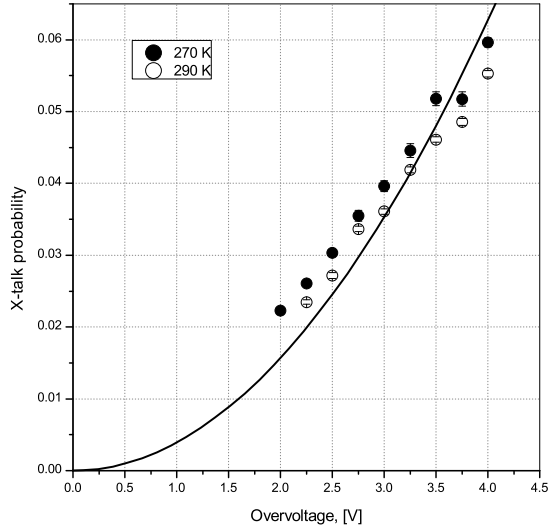
15

Рис. 19. The dependence of the cross–talk probability on an overvoltage at a fixed temperature for Hamamatsu S13360-3050CS. The data were approximated by a quadratic function.
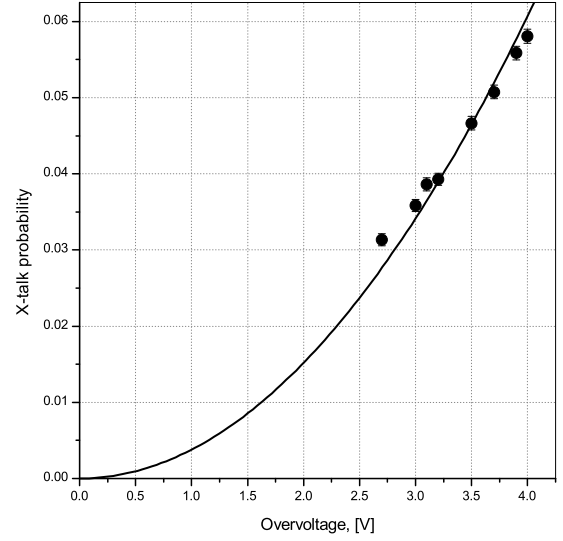
Рис. 20. The dependence of the cross–talk probability on an overvoltage at a fixed temperature for KETEK PM1125NS-SB0. The data were approximated by a quadratic function.

The time constants τ_s and τ_f at a given measurement accuracy are independent on an overvoltage.

6. Conclusions

In the work were described the algorithms for measurement the breakdown voltage, dark noise, probabilities for cross-talk and after-pulsing and after-pulsing time constants for three SiPMs types: KETEK PM1125NS-SB0, Hamamatsu S10362-11-100C and Hamamatsu S13360-3050CS.

An offline signal processing was performed by the pulse approximation with reconstruction of amplitudes and start times to find these parameters. Besides the algorithm used, there are three methods. The first - the measurement of the pulse rate depending on the amplitude threshold. The second - the integration a signal at a certain time interval and finding a number of events in the peaks. The third - the signal deconvolution and an approximation of the pulse interval spectrum. The first two methods are rather simple and can be used in an online analysis but they have a serious drawback - after-pulsing probabilities and after-pulsing time constants can't be found. The third method, and the method used in this study require large computing power, however, allow us to find after-pulsing parameters.

At achieved measurement accuracy in the temperature range from 0 to $20C^\circ$ the
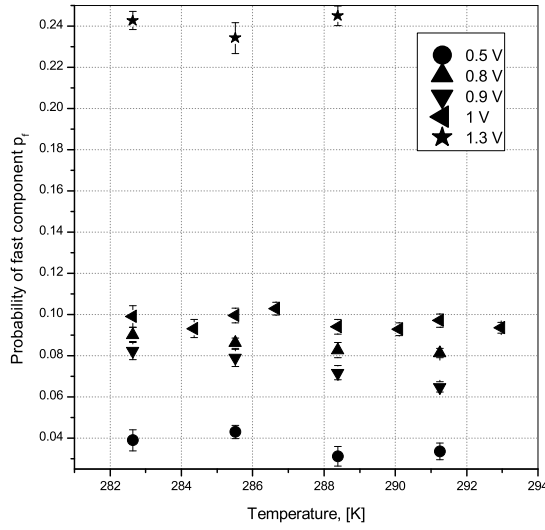
16

Рис. 21. The dependence of the fast component probability p_f for an after-pulse on a temperature at a fixed overvoltage for Hamamatsu S10362-11-100C.
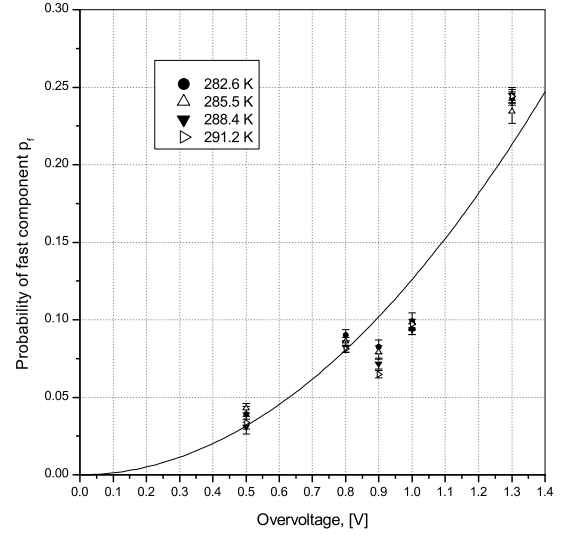
Рис. 22. The dependence of the fast component probability p_f for an after-pulse on an overvoltage at a fixed temperature for Hamamatsu S10362-11-100C. The data were approximated by a quadratic function.

cross-talk probability, after-pulsing probabilities and after-pulsing time constants are independent on a temperature. SiPMs were checked for compliance with the four neighbors model. All three types of SiPMs have model discrepancy less than 10%.

The cross-talk probability for Hamamatsu S10362-11-100C at an operating overvoltage (1 V) is about 12%, for Hamamatsu S13360-3050CS and KETEK PM1125NS-SB0 (an operating overvoltage is 4 V) is about 6%. After-pulsing probabilities for Hamamatsu S10362-11-100C at an operating overvoltage is about 10% (fast component) и 15% (slow component). For Hamamatsu S13360-3050CS and KETEK PM1125NS-SB0 because of the small statistics it was studied only the fast component, which is about 10%. After-pulsing time constants for Hamamatsu S10362-11-100C are about 35 ns (fast component) and 170 ns (slow component), for Hamamatsu S13360-3050CS - 9 ns, for KETEK PM1125NS-SB0 - 28 ns. Dark noise rate for Hamamatsu S10362-11-100C at an operating overvoltage and 20 $°C$ temperature is about 300 kHz/mm^2, for Hamamatsu S13360-3050CS - 30 kHz/mm^2, for KETEK PM1125NS-SB0 - 80 kHz/mm^2.

Thus, on the basis of the experiments we can conclude that the best candidate for use in counting detectors among the studied SiPMs is Hamamatsu S13360-3050CS which has lower dark noise rate and the least after-pulsing time constants.
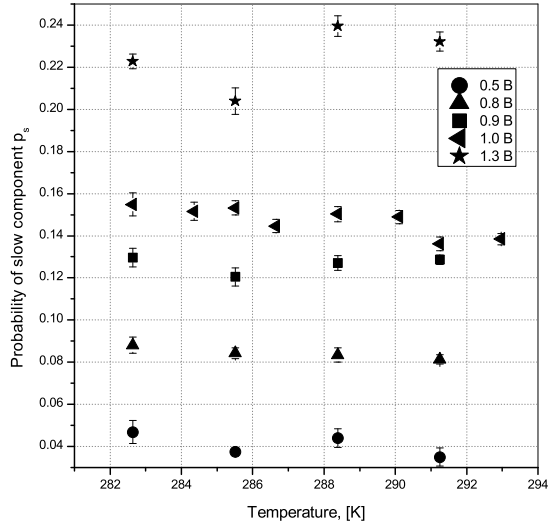
Рис. 23. The dependence of the slow component probability p_s for an after-pulse on a temperature at a fixed overvoltage for Hamamatsu S10362-11-100C.
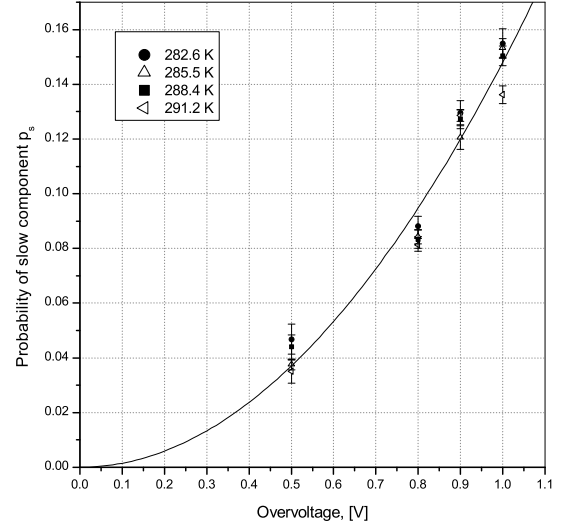

Рис. 24. The dependence of the slow component probability p_s for an after-pulse on an overvoltage at a fixed temperature for Hamamatsu S10362-11-100C. The data were approximated by a quadratic function.
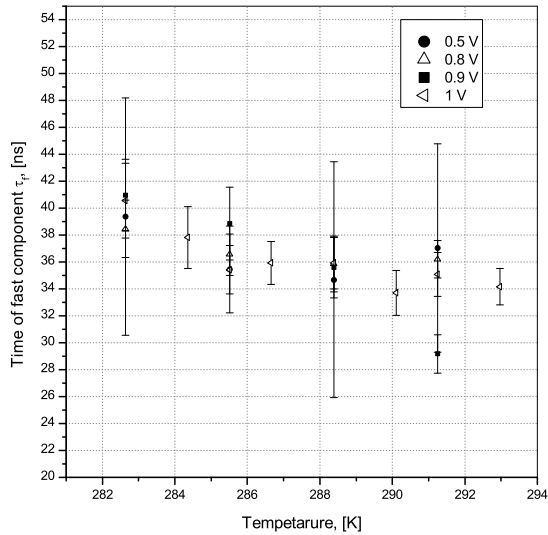

Рис. 25. The dependence of the fast time constant τ_f for an after-pulse on a temperature at a fixed overvoltage for Hamamatsu S10362-11-100C.
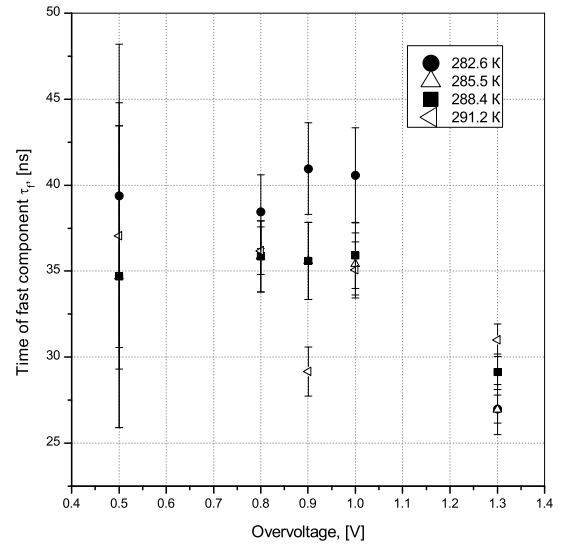
Рис. 26. The dependence of the fast time constant τ_f for an after-pulse on an overvoltage at a fixed temperature for Hamamatsu S10362-11-100C.
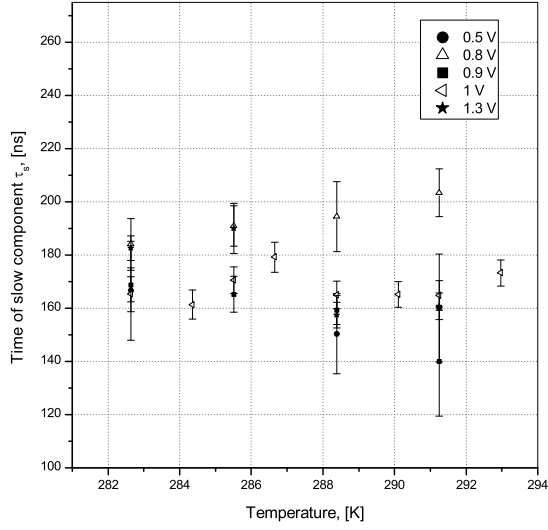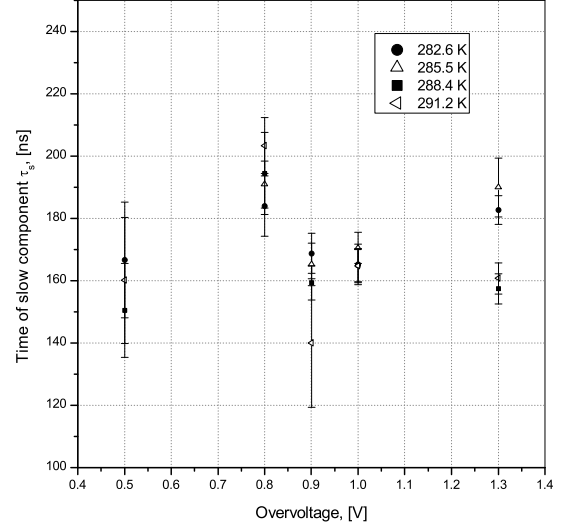
Рис. 27. The dependence of the slow time constant τ_s for an after-pulse on a temperature at a fixed overvoltage for Hamamatsu S10362-11-100C.

Рис. 28. The dependence of the slow time constant τ_s for an after-pulse on a overvoltage at a fixed temperature for Hamamatsu S10362-11-100C.
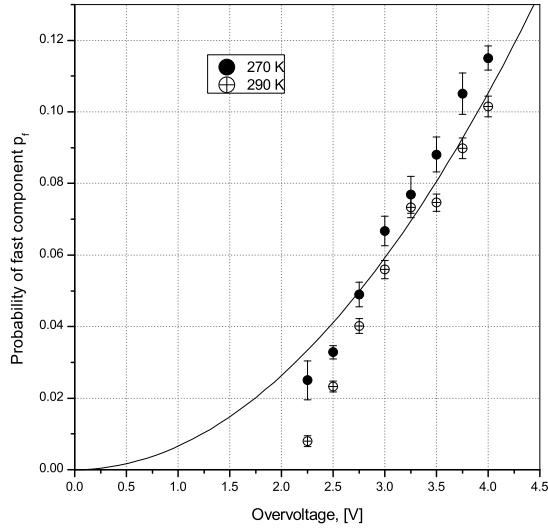

Рис. 29. The dependence of the fast component probability p_f for an after-pulse on an overvoltage at a fixed temperature for Hamamatsu S13360-3050CS. The data were approximated by a quadratic function.
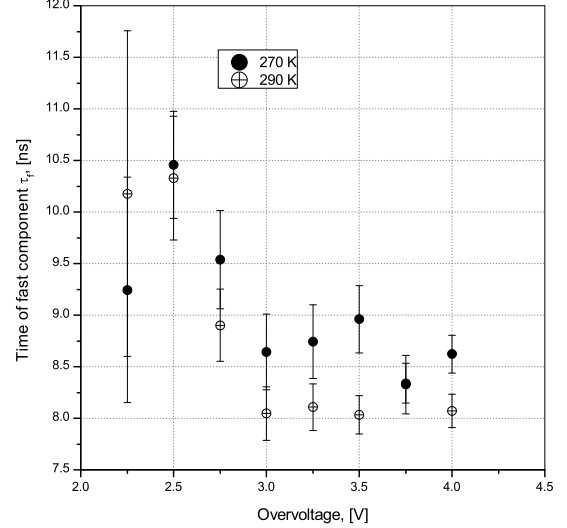

Рис. 30. The dependence of the fast time constant τ_f for an after-pulse on an overvoltage at a fixed temperature for Hamamatsu S13360-3050CS.
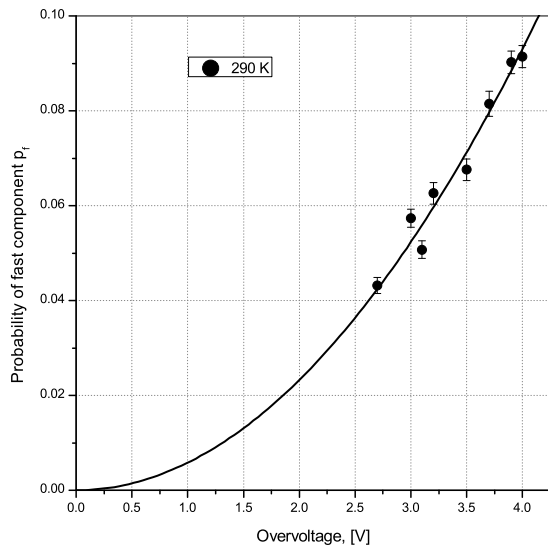
Рис. 31. The dependence of the fast component probability p_f for an after-pulse on an overvoltage at a fixed temperature for KETEK PM1125NS-SB0. The data were approximated by a quadratic function.
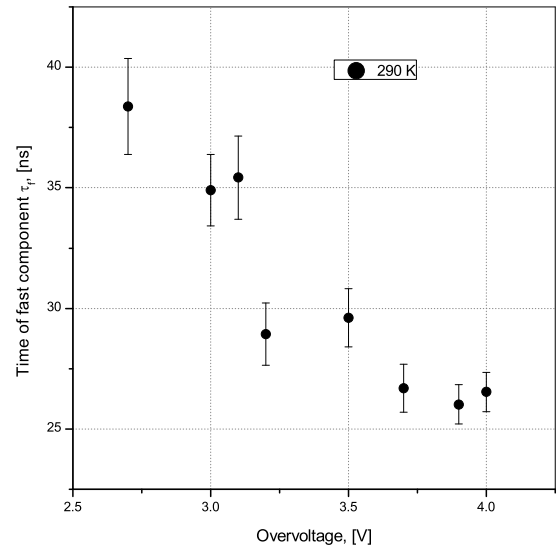

Рис. 32. The dependence of the fast time constant τ_f for an after-pulse on an overvoltage at a fixed temperature for KETEK PM1125NS-SB0.

Список литературы

[1] E.A. Babichev et al., SiPM based photon counting detector for scanning digital radiography, JINST 10 (2015) C03002

[2] P. Dorosz et al., Silicon Photomultiplier's Gain Stabilization by Bias Correction for Compensation of the Temperature Fluctuations, , Nucl. Instrum. Meth. A 718 (2013) pp. 202–204

[3] N. Dinu et al., Temperature and Bias Voltage Dependence of the MPPC Detectors, IEEE Oct. 30 2010-Nov. 6 2010 pp.215 - 219

[4] Marco Ramilli, Characterization of SiPM: temperature dependencies, IEEE 19-25 Oct. 2008 pp. 2467 - 2470

[5] P.K. Lightfoot et al., Characterisation of a silicon photomultiplier device for applications in liquid argon based neutrino physics and dark matter searches, JINST 3 (2008) P10001

[6] Patrick Eckert et al., Characterisation Studies of Silicon Photomultipliers, Nucl. Instrum. Meth. A 620 (2010) pp. 217–226

[7] L. Gallego et al., Modeling crosstalk in silicon photomultipliers, Nucl. Instrum. Meth. A 787 (2015) pp. 153–156

[8] A. Vacheretc et al., Characterization and Simulation of the Response of Multi Pixel Photon Counters to Low Light Levels, Nucl. Instrum. Meth. A 656 (2011) pp. 69-83

[9] Y. Du et al., After-pulsing and cross-talk in multi-pixel photon counters, Nucl. Instr. and Meth. A 596 (2008) pp. 396-401

[10] Fabrice Retiere, Using MPPCs for T2K Fine Grain Detector, PoS PD07 (2006) 017

[11] J. Rosado et al., Modeling crosstalk and afterpulsing in silicon photomultipliers, Nucl. Instr. and Meth. A 787 (2015) pp. 153–156

[12] Daniel Orme et al., Measurement of PDE of MPPC with different wavelengths of light, PoS PD09 (2009) 019